The EMBO Journal Vol. 21 No. 24 pp. 6935–6943, 2002

F-actin-like filaments formed by plasmid segregation protein ParM

Fusinita van den Ent, Jakob Møller-Jensen[1], Linda A.Amos, Kenn Gerdes[1] and Jan Löwe[2]

MRC Laboratory of Molecular Biology, Hills Road, Cambridge CB2 2QH, UK and [1]Department of Biochemistry and Molecular Biology, University of Southern Denmark, DK-5230 Odense M, Denmark

[2]Corresponding author
e-mail: jyl@mrc-lmb.cam.ac.uk

F.van den Ent and J.Møller-Jensen contributed equally to this work

It was the general belief that DNA partitioning in prokaryotes is independent of a cytoskeletal structure, which in eukaryotic cells is indispensable for DNA segregation. Recently, however, immunofluorescence microscopy revealed highly dynamic, filamentous structures along the longitudinal axis of *Escherichia coli* formed by ParM, a plasmid-encoded protein required for accurate segregation of low-copy-number plasmid R1. We show here that ParM polymerizes into double helical protofilaments with a longitudinal repeat similar to filamentous actin (F-actin) and MreB filaments that maintain the cell shape of non-spherical bacteria. The crystal structure of ParM with and without ADP demonstrates that it is a member of the actin family of proteins and shows a domain movement of 25° upon nucleotide binding. Furthermore, the crystal structure of ParM reveals major differences in the protofilament interface compared with F-actin, despite the similar arrangement of the subunits within the filaments. Thus, there is now evidence for cytoskeletal structures, formed by actin-like filaments that are involved in plasmid partitioning in *E.coli*.

Keywords: DNA partitioning/F-actin/MreB/ParM

Introduction

The mitotic apparatus in eukaryotes is instrumental for the correct distribution of DNA among progeny cells (reviewed in Heald, 2000). It has long been thought that DNA segregation in bacteria is independent of cytoskeletal structures such as the mitotic spindle. However, new data on the rapid and direct translocation of newly replicated plasmids and origins of replication on bacterial chromosomes suggest a force-generating process (Niki and Hiraga, 1998; Jensen and Shapiro, 1999; Sharpe and Errington, 1999; Gordon and Wright, 2000). Although little is known about the molecular detail underlying bacterial DNA partitioning, recent studies on plasmid segregation have provided the first clues to a possible mechanism. Low-copy-number plasmids encode partitioning genes (*par*) (Austin and Abeles, 1983; Ogura and Hiraga, 1983; Gerdes *et al*., 1985) that are required for faithful segregation of the plasmid before cell division (for a recent review, see Gerdes *et al*., 2000). More recently, orthologues of the *par* genes were identified on bacterial chromosomes (Ogasawara and Yoshikawa, 1992; Ireton *et al*., 1994; Mohl and Gober, 1997). The directional movement and positioning of newly replicated plasmids and chromosomes are dependent on the *par* loci (for recent reviews, see Jensen and Shapiro, 1999; Sharpe and Errington, 1999; Gerdes *et al*., 2000; Møller-Jensen *et al*., 2000). All known *par* loci encode three components: a *cis*-acting centromere-like DNA sequence and two *trans*-acting proteins that together form a nucleoprotein complex (partitioning complex). Transcription of the *par* genes is autoregulated by binding of one or both *trans*-acting proteins to the *par* operon promoter region. The centromere-like region interacts with one of the *trans*-acting proteins. The other protein component of the partitioning complex is an ATPase that either belongs to the actin family of proteins, as determined by weak sequence homology, or is a Walker-type ATPase (Koonin, 1993). In the case of the nucleoprotein complex in *Escherichia coli* that actively segregates the low-copy-number plasmid R1, the ATPase is ParM (also known as StbA), the centromere-binding protein is ParR and the centromeric region is *parC*. Two plasmid molecules are paired at their centromeric regions through the interaction with ParR (Jensen *et al*., 1998). ParM interacts with the ParR–*parC* complex that stimulates its ATPase activity (Jensen and Gerdes, 1997; Møller-Jensen *et al*., 2002). A sequence database search revealed that the active site of ParM matches the consensus sequence of the actin family of proteins (Bork *et al*., 1992). However, this does not necessarily imply that the role of ParM is related to that of actin, as bacterial relatives of the actin superfamily of proteins have very diverse functions. Bacterial proteins that have been identified as belonging to the actin family of proteins include DnaK, FtsA, MreB and ParM. DnaK, whose ATPase domain is structurally related to actin, helps other proteins in the folding process (reviewed in Netzer and Hartl, 1998). The bacterial cell division protein FtsA is crucial for cytokinesis (Rothfield *et al*., 1999), but its precise role is not yet understood. Although the overall three-dimensional architecture of FtsA clearly indicates that it is a member of the actin family of proteins (van den Ent and Löwe, 2000), the second subdomain has a unique position, which probably prevents actin-like filament formation. The propensity of MreB to self-assemble into actin-like filaments, which, like F-actin, are indispensable for maintenance of cell shape has been the primary reason to regard MreB as a true bacterial actin homologue (Jones *et al*., 2001; van den Ent *et al*., 2001a).

In the past, cell division protein FtsZ was identified as the bacterial homologue of eukaryotic tubulin (Löwe and

Amos, 1998). FtsZ polymerizes in an analogous fashion to tubulin and forms a ring-like structure that mediates bacterial cell division (Bi and Lutkenhaus, 1991; Addinall and Lutkenhaus, 1996; Erickson, 1998; Löwe and Amos, 1999). The existence in bacteria of these cytoskeletal structures comprising actin and tubulin homologues has eliminated an apparent fundamental difference between prokayotes and eukaryotes (van den Ent *et al*., 2001b).

The last predicted bacterial relative of the actin family of proteins in *E.coli*, ParM, has been investigated here. If a clear structural similarity between ParM and actin could be established, the role of bacterial cytoskeletal structures could be extended to DNA segregation. Recently, immunofluorescence microscopy showed that ParM of plasmid R1 forms highly dynamic, filamentous structures extending along the longitudinal axis of *E.coli* that are essential for the DNA partitioning process (Møller-Jensen *et al*., 2002). Also, *in vitro*, it has been shown that ParM self-assembles in an ATP-dependent manner (Møller-Jensen *et al*., 2002).

Are these filamentous structures actin-like filaments? Here, we show by electron microscope analyses that ParM self-assembles into double helical protofilaments with a longitudinal repeat similar to actin and MreB. The elucidation of the crystal structure of ParM demonstrates the structural homology to actin and MreB at the atomic level. The structure of ParM in both the unbound and the ADP-bound state was determined. A large rigid body movement between the two domains upon nucleotide binding is evident. Thus, the structural and functional properties of ParM imply a role for dynamic actin-like structures in plasmid R1 segregation.

Results and discussion

How actin like are ParM filaments?

ParM self-assembles into filaments in the presence of ATP, ATPγS or AMPPNP, but not in the presence of ADP (Møller-Jensen *et al*., 2002). To investigate the nature of these filaments, negatively stained samples were examined under the electron microscope. As shown in Figure 1A, the majority of the protein polymerized into long, straight filaments. A closer look at those polymers revealed that they consist of two protofilaments that gently twist around each other, as shown at higher magnification (Figure 1B). This becomes even clearer in the filtered images (Figure 2B and C). The Fourier transform of the straightened polymer (Figure 2D) contains layer lines that form a pattern similar to that of eukaryotic filamentous actin (F-actin) and imply a regular helical arrangement (Table I). This is in contrast to the arrangement of the subunits of MreB (van den Ent *et al*., 2001a), which, *in vitro*, self-assemble into more or less straight polymers. The layer line at 300 Å indicates the crossover distance of the paired ParM protofilaments. The crossover distance in F-actin is variable, with an average length of 360 Å (Galkin *et al*., 2002). The upper group of layer lines indicate a longitudinal subunit spacing of 49 Å, which is very close to the 51 Å spacing found in MreB (van den Ent *et al*., 2001a) and the 55 Å spacing in F-actin (Holmes *et al*., 1990).

Our electron microscope analyses show that ParM filaments can be regarded as a two-start helix with a twist

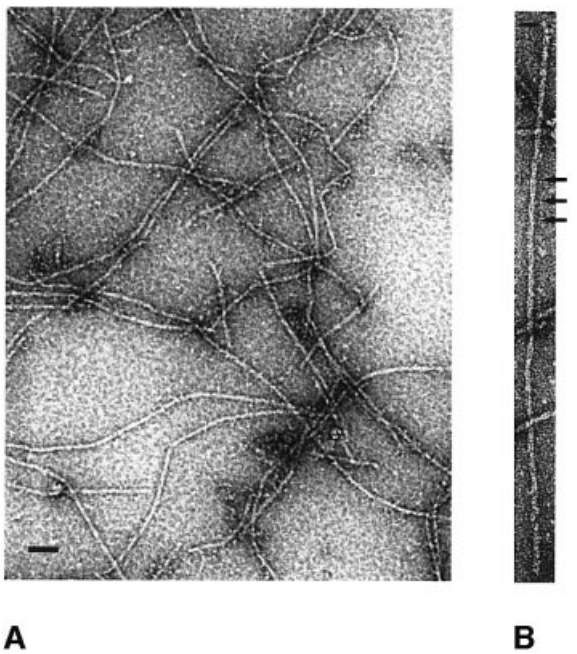

Fig. 1. Electron micrographs of negatively stained ParM filaments. (**A**) Typical overview of a grid containing ParM filaments. The protein (1 mg/ml) was incubated in polymerization buffer (30 mM Tris–HCl pH 7.5, 100 mM KCl, 2 mM $MgCl_2$, 1 mM DTT) in the presence of 2 mM ATPγS for 5 min at room temperature. Scale bar, 100 nm. (**B**) ParM filament at higher magnification, showing the helical arrangement of the protofilaments. The crossovers are indicated by arrows. Scale bar, 100 nm.

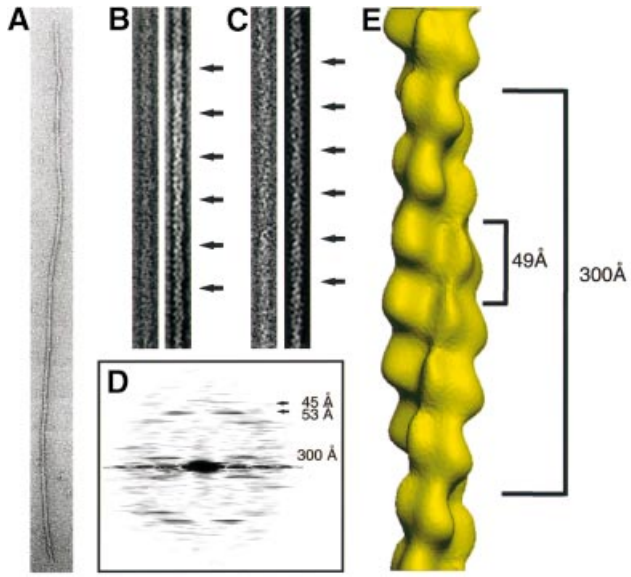

Fig. 2. Analysis of electron micrographs of ParM. (**A**) A typical ParM filament before straightening. (**B** and **C**) The right panel shows the filtered image of the straightened filament in the left panel. The arrows indicate the crossovers of the two protofilaments. (**D**) Averaged diffraction pattern from six straightened filaments. The layer lines at 45 and 53 Å are derived from one-start left- and right-handed helices. The two-start helix produces the layer line of 300 Å. (**E**) Three-dimensional reconstruction. The distance of 49 Å between the subunits is the average between the layer lines from the one-start helices. The crossover distance of 300 Å is shown on the right.

slightly tighter than that of F-actin and a slightly shorter longitudinal spacing of 49 Å (Figure 2E). A helical rather than a straight arrangement of the subunits in ParM filaments should increase the strength of the filaments and provides an intrinsic limitation for lateral growth.

How actin like is ParM?

Despite the homology of ParM protofilaments to F-actin, evidence that the proteins are structurally similar at the atomic level has still to be obtained. To determine the three-dimensional structure of ParM, orthorhombic and tetragonal crystals were grown (see Materials and methods). The structure of selenomethionine (SeMet)-substituted ParM was solved by multiple anomalous dispersion (MAD; Table II). The structure of the native crystal (space group $P2_12_12$) was determined to 2.3 Å resolution using the model of SeMet-substituted ParM. The tetragonal ADP-bound crystals (space group $P4_1$) diffracted to 2.0 Å. The crystals were perfectly twinned, which was facilitated by identical *a*- and *b*-axes, and hence appeared to have point group 422. The structure of the ADP-bound form was solved by molecular replacement and Patterson correlation refinement to overcome the large conformational shift between the two states of ParM. The model was refined using CNS1.1 (Brünger *et al*., 1998), assuming a twinning fraction of 50%. Refinement statistics are summarized in Table III.

The elucidation of the crystal structure of ParM revealed that it is indeed closely related to actin and MreB. ParM has the characteristic fold of the actin family of proteins (Figure 3): two domains (I and II) with a nucleotide-binding pocket in the interdomain cleft (Kabsch and Holmes, 1995). Each domain is divided into two subdomains (A and B). The larger subdomains (IA and IIA) share a common fold that consists of a five-strand β-sheet surrounded by three α-helices. In general, the two smaller subdomains are more variable in size and structure.

Once ParM binds ADP, the interdomain cleft closes as domains I and II approach each other as rigid bodies (Figure 3). The domain movement upon ADP binding is ~25°, with the connecting helix H5 (residues 152–154) acting as a mechanical hinge (as determined with the program Dyndom; Hayward *et al*., 1997). The rigid body movement validates the original nomenclature that divided the actin fold into two main domains (Bork *et al*., 1992), rather than the four domains conventionally assigned. The movement of the domains between nucleotide-free and -bound actin is smaller than the 25° rotation seen in ParM based on the nucleotide-free Arp2/3 and the structures of actin with nucleotide (Schutt *et al*., 1993; Otterbein *et al*., 2001; Robinson *et al*., 2001; Sablin *et al*., 2002). The domain movements in ParM are similar in magnitude to what has been suggested to occur within a tilted state of F-actin (Galkin *et al*., 2002).

ParM and the actin family of proteins

A three-dimensional similarity search (Holm and Sander, 1993) with the structure of ParM revealed MreB and actin as closest relatives (r.m.s.d. of 3.3 Å over 261 C_α atoms for actin; r.m.s.d. of 3.7 Å over 255 C_α atoms for MreB; see the legend to Figure 4). The other members of the actin family of proteins, HSC70 and FtsA, are more distantly related to ParM. The N-terminal region of chaperone HSC70 [constitutive Hsp70 protein, Protein Data Bank (PDB) entry 1ba1; Flaherty *et al*., 1990] is very similar to actin, MreB and ParM (it superimposes on ParM with an r.m.s.d. of 3.1 Å over 267 C_α atoms and a *Z*-score of 21.4), but the C-terminal region is unrelated to the actin family of proteins. Bacterial cell division protein FtsA has the second subdomain located at the opposite side of subdomain IA (van den Ent and Löwe, 2000). The remaining part of the protein superimposes reasonably

Table I. Electron microscopy data on filament-forming actin-like proteins

	F-actin[a]	ParM[b]	MreB[c]
Protofilament repeat (Å)	55	49	51
Crossover repeat (Å)	~360	~300	
Subunits/repeat	13	12.5	
Rotation (°)	166.2	165.6	

[a]The values for F-actin are the average for uncomplexed muscle and yeast actin (Galkin *et al*., 2002).
[b]As described in this paper.
[c]See van den Ent *et al*. (2001a). Since the observed filaments of MreB are straight, only the longitudinal distance between the subunits is given.

Table II. Crystallographic data

$P2_12_12$:	$P4_1$:
a = 117.68 Å	$a = b$ = 64.71 Å
b = 72.47 Å	c = 199.71 Å
c = 87.56 Å	twinning fraction 50%

Crystal	λ (Å)	SG	Resolution (Å)	$I/\sigma I$[a]	R_m[b]	Multiplicity[c]
PEAK	0.9792	$P2_12_12$	2.6	22.6 (9.6)	0.057	6.3
INFL	0.9798	$P2_12_12$	2.6	21.8 (8.4)	0.060	6.3
HREM	0.9393	$P2_12_12$	2.6	19.1 (7.2)	0.082	6.3
APO	0.9393	$P2_12_12$	2.3	14.8 (3.4)	0.064	3.1
ADP	0.9600	$P4_1$	2.0	15.4 (4.6)	0.064	4.1

[a]Signal-to-noise ratio of intensities, highest resolution bin in parentheses.
[b]$R_m = \Sigma_h\Sigma_i|I(h,i) - I(h)|/\Sigma_h\Sigma_i I(h,i)$, where $I(h,i)$ are symmetry-related intensities and $I(h)$ is the mean intensity of the reflection with unique index h.
[c]Multiplicity for unique reflections; for MAD datasets $I(+)$ and $I(-)$ are kept separate. Correlation coefficients of anomalous differences at different wavelengths for MAD experiment: PEAK versus INFL: 0.48; PEAK versus HREM: 0.59; INFL versus HREM: 0.33.

Table III. Refinement statistics

	APO	ADP
Residues	1: 1–320; 2: 1–211, 217–319	A: 1–63; 68–320 B: 1–63; 68–320
Water, cofactor	282	370, Mg-ADP
Resolution (Å)	2.3	2.0
Twinning fraction[a]		0.50
R-factor, R_{free}[b]	0.217, 0.266	0.221, 0.252
B average[c] (Å^2)	42.7	37.6
Geometry bonds (Å)/angles (°)[d]	0.006, 1.193	0.008, 1.381
Ramachandran[e] (%)	88.5/0.0	90.8/0.0
PDB ID[f]	1MWK	1MWM

[a]Twinning fraction as used in refinement, operator h, –k, –l.
[b]Five per cent of reflections were randomly selected for determination of the free *R*-factor (taking twinning into account where appropriate), prior to any refinement.
[c]Temperature factors averaged for all atoms.
[d]R.m.s.ds from ideal geometry for bond lengths and restraint angles (Engh and Huber, 1991).
[e]Percentage of residues in the 'most favoured region' of the Ramachandran plot and percentage of outliers (PROCHECK; Laskowski *et al*., 1993).
[f]PDB identifiers for coordinates and structure factors, respectively.

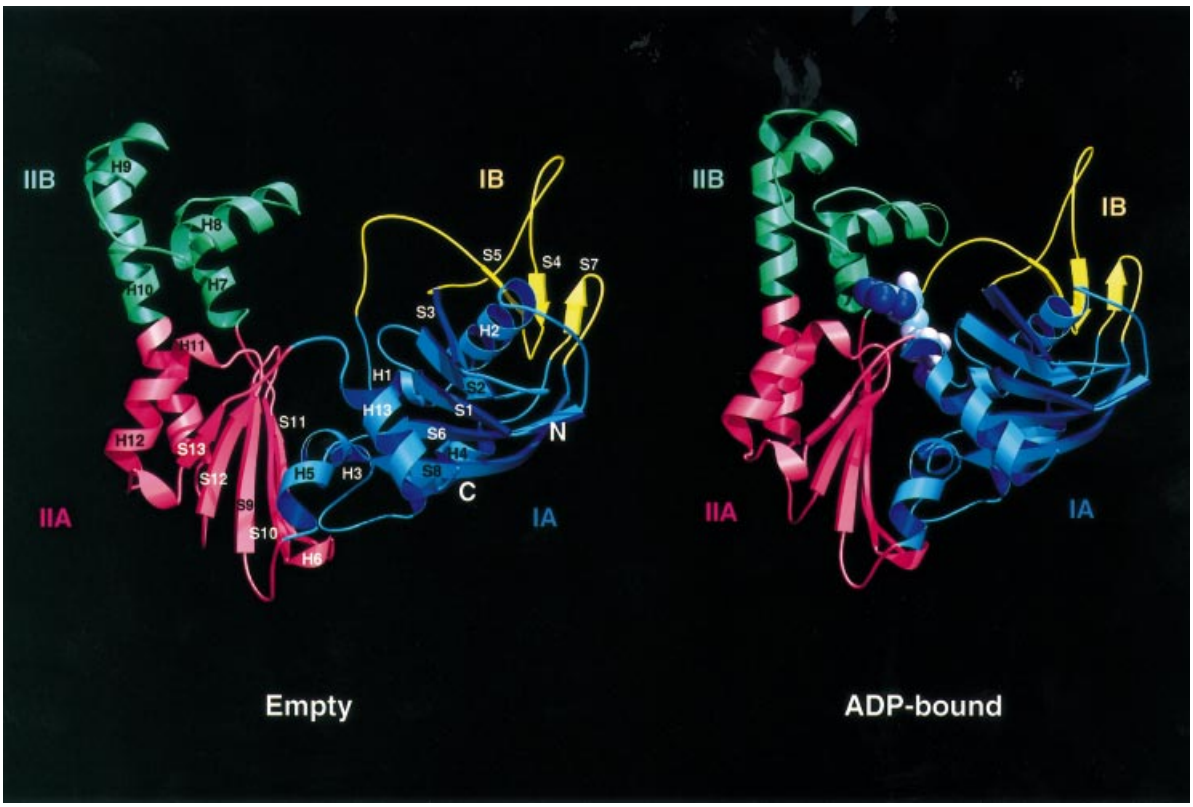

Fig. 3. Ribbon plot of ParM in the empty form (left) and the ADP-containing form (right). ParM, as a member of the actin family of proteins, consists of two domains (I and II), which are divided into two subdomains (A and B). ADP binds in the interdomain cleft, which closes upon nucleotide binding through a rigid body movement of domains I and II. Images were created with MOLSCRIPT and RASTER3D (Kraulis, 1991; Merritt and Bacon, 1997).

well on ParM (r.m.s.d. of 3.3 Å over 248 C_α atoms and a *Z*-score of 19).

Despite the structural similarity between ParM and actin/MreB, the sequence identity is low. A structure-based sequence alignment between ParM and actin (see Supplementary data available at *The EMBO Journal* Online) shows that <12% of the amino acids in ParM are identical to actin. The sequence similarity is equally low between ParM and MreB (11%), and only slightly higher between MreB and actin (15%; van den Ent *et al*., 2001a). The highest conservation is found in the residues that line the nucleotide-binding pocket, an observation that led to the prediction that ParM and MreB belong to the actin family of proteins (Bork *et al*., 1992). The active site of ParM containing Mg-ADP (see Supplementary data) can be superimposed on that of ADP-bound actin (Otterbein *et al*., 2001) with the main domains in approximately similar relative orientations. In both proteins, the magne-

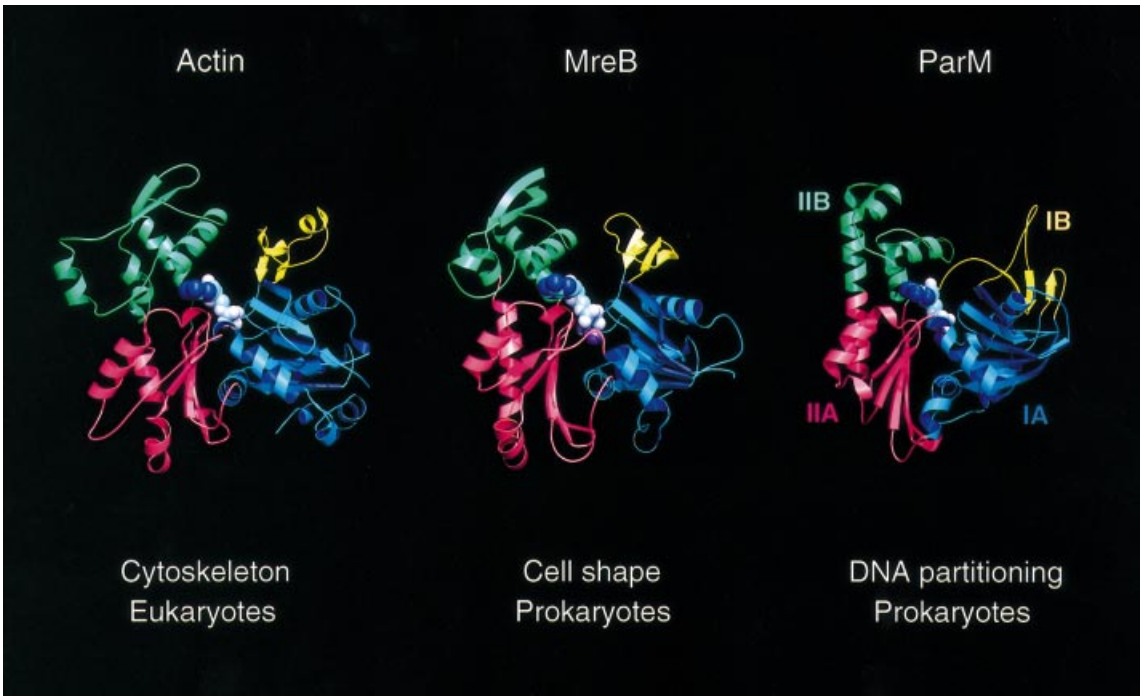

Fig. 4. Comparison of filament-forming proteins of the actin family of proteins. Eukaryotic actin is shown here in the ADP form (PDB entry 1J6Z). MreB is involved in the maintenance of cell shape in non-spherical bacteria (here shown in complex with AMPPNP; PDB entry 1JCG). ParM forms actin-like filaments in *E.coli* that are required for segregation of plasmid R1. It is shown here in the ADP form. Colour codes are the same as for Figure 3 (with subdomain IA in blue, IB in yellow, IIA in red and IIB in green). Subdomains IA, IB, IIA and IIB correspond to subdomains 1, 2, 3 and 4 in actin. ParM can be superimposed on 261 C_α atoms of actin (PDB entry 1yag-A) with an r.m.s.d. of 3.3 Å and a *Z*-score of 20.4. Similarly, it can be superimposed on MreB (PDB entry 1JCF) with an r.m.s.d. of 3.7 Å, for 255 C_α atoms, and a *Z*-score of 20.3 (Holm and Sander, 1993). As comparison, 310 C_α atoms of MreB superimpose on actin with an r.m.s.d. of 3.7 Å and a *Z*-score of 29.2 (van den Ent *et al*., 2001a).

sium ion is coordinated via an aspartate. Mutagenesis of this aspartate in ParM (D170A or D170E) impairs plasmid segregation (Jensen and Gerdes, 1997). Although the mutant protein still polymerizes, the filaments are no longer dynamic (Møller-Jensen *et al*., 2002). This indicates that the disassembly of the filaments requires ATP hydrolysis, whereas filament formation, as such, is independent of nucleotide hydrolysis.

Although the overall fold of ParM resembles actin (Figure 4), ParM has some unique features, which were unexpected for a protein whose filaments are almost indistinguishable from F-actin. Surprisingly, the differences are in regions that are involved in protofilament contacts. The first major difference is in subdomain IB. A long loop at the beginning of this subdomain is the most obvious difference. It partially overlaps with the DNase I-binding loop in actin. However, the loop in ParM does not change conformation upon ADP binding, which is in contrast to the DNase I-binding loop in actin (Kabsch *et al*., 1990; Egelman, 2001; Otterbein *et al*., 2001). Moreover, the overall fold of subdomain IB is unique for ParM. It is composed of a single sheet (7p4a5p) and lacks the α-helix found in the equivalent subdomains of MreB and ADP-bound actin. Unexpectedly, the third strand, S7, in ParM comes from an insertion in subdomain IA, a peculiarity not seen in any other member of the actin family. It has been shown for actin that subdomain IB adopts various conformations, dependent on the nucleotide state of the protein and the divalent cation bound by the active site (Belmont *et al*., 1999; Otterbein *et al*., 2001; Sablin *et al*., 2002). In the initial structure of actin co-crystallized with DNase I, the conformation of this subdomain is very similar to that of MreB (5a4p6a), with the DNase I-binding loop inserted between strands S4 and S5.

The two other major differences between ParM and actin/MreB may explain the smaller spacing between the subunits in the ParM protofilament. First, MreB and actin have a two-stranded β-sheet on top of the α-helices of subdomain IIB (Figure 4). The β-sheet makes intersubunit contacts along the protofilament of MreB, as has been observed in the crystal structure (van den Ent *et al*., 2001a), and is presumably also important for the assembly of F-actin (Holmes *et al*., 1990; Chen *et al*., 1993; Otterbein *et al*., 2001). In ParM, the β-sheet is replaced by a short helix (H9), a small loop and part of helix H10. Secondly, a short loop in ParM (connecting helix H10 and strand S12) substitutes a substantial helix in actin/MreB at the bottom of domain IIA (see the structure-based sequence alignment in Supplementary data), a helix that also forms part of the interface between the subunits of the MreB protofilament. The lack of this helix in subdomain IIA and the two-stranded β-sheet in subdomain IIB makes ParM shorter than MreB and actin.

Actin has an insertion in the long helix connecting subdomains IIA and IIB, named the hydrophobic plug. This loop is thought to hold the protofilaments together (Holmes *et al*., 1990; Chen *et al*., 1993). Since the hydrophobic plug is absent in MreB, it was speculated that it might actually induce the twist in F-actin. However, ParM also lacks the plug. Apparently, interactions other

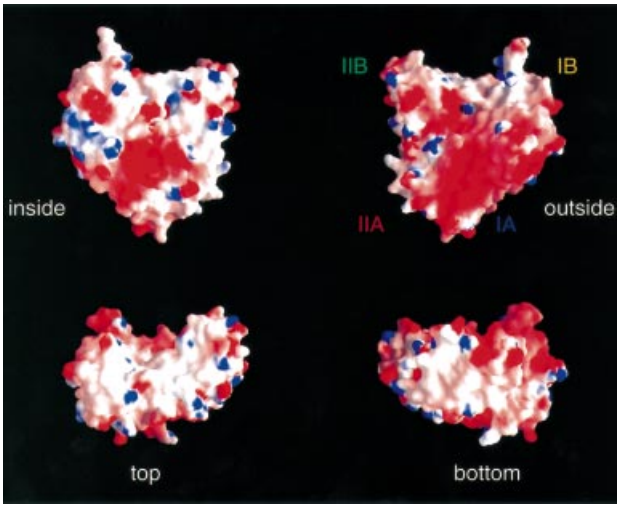

Fig. 5. Surface charge distribution of ParM. The electrostatic potential [–6 kT (red) to +6 kT (blue)] is plotted onto the surface of ParM. The plots shown are a view from the outside of the filaments ('outside'), and a view facing the second protofilament ('inside'); 'top' and 'bottom' show the surface of the subunits after a 90° rotation around the *x*-axis, with respect to the plots in the upper half of the figure. Subdomains are labelled as in Figure 3. The figure was prepared using GRASP (Nicholls *et al*., 1991).

than the hydrophobic plug induce the twist and stabilize the filaments in ParM.

Atomic model of a ParM filament

Although the current resolution of the electron microscopy images is too low to show a ParM filament in detail, a putative model can be built based on the surface charge distribution of ParM and its similarities to actin/MreB.

In the crystals of MreB, the protein is assembled into filaments, providing an accurate picture of the arrangement of the subunits in the protofilament for actin-like proteins and actin itself (van den Ent *et al*., 2001a). We assumed that the subunit arrangement in the ParM protofilament is analogous to MreB, therefore head to tail, and this matches with the surface charge distribution (Figure 5). The long, hydrophobic loop in subdomain IB (including residues 38–41) could slide into a hydrophobic pocket at the bottom of subdomain IA. From Figure 5, it is obvious that one of the flat surfaces is particularly acidic (right top corner of Figure 5). This region probably forms the outside of the filament, as has been postulated for actin. The inner surface is predominantly hydrophobic, which is expected for a protein–protein interface. Taking those assumptions into account, the crystal structure of ParM was assembled into a helical filament and superimposed on the density derived from the electron microscopy data (Figure 6). The polarity is fixed with the pointed end at the top compared with myosin-decorated F-actin, assuming that the same side of ParM forms the inside of the filament when compared with F-actin. As for the model of F-actin, it is currently not possible to accurately assign residues involved in the protofilament interface, because of the low-resolution data. However, it is obvious from both the structure-based sequence alignment between ParM and actin, and the variation in topology, that the interfaces must be different. The low degree of conservation of the

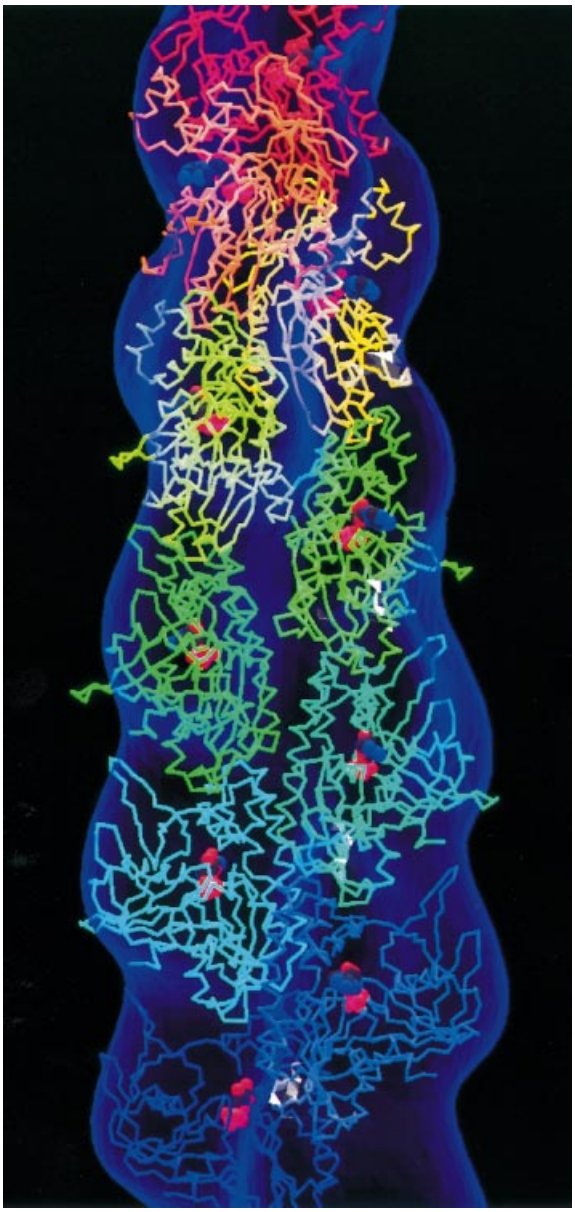

Fig. 6. Docking the crystal structure of ParM into the density derived from the negatively stained ParM filaments. ParM subunits are assembled head to tail into a protofilament. Each successive subunit is rotated by ~166° and translated by 24.5 Å to create a helical filament. Every molecule of ParM is complexed with ADP and has a different rainbow colour, turning red toward the pointed end. The figure was created with MOLSCRIPT (Kraulis, 1991).

residues in the protofilament interface was also noticed when the filaments of MreB and actin were compared, and co-evolution of residues at either site of the interface was proposed (van den Ent *et al*., 2001a).

Actin-like filaments are involved in DNA partitioning

The elucidation of the ParM structure demonstrates that it is a close relative of the filamentous proteins MreB and actin. The most obvious differences are in regions that are likely to be involved in protofilament contacts. An amazing discrepancy between the two prokaryotic actin-like proteins is their propensity to form either straight (MreB) or twisted filaments (ParM) *in vitro*. Filament

formation requires binding of ATP or a non-hydrolysable ATP analogue (van den Ent *et al*., 2001a; Møller-Jensen *et al*., 2002). ATP hydrolysis by ParM promotes filament dynamics presumably through a mechanism similar to that of F-actin, in which it is assumed that the energy released from the hydrolysis of ATP induces a conformational change in the protein, thereby weakening the bonds between the subunits in the filament. Subsequently, this would lead to depolymerization. An exceptional property of ParM is that it couples ATP hydrolysis to DNA partitioning in bacteria.

The actin-like properties of ParM explain its ability to form dynamic, fibrous structures observed by immunofluorescence microscopy (Møller-Jensen *et al*., 2002). It remains to be determined whether the mechanism used to carry the newly replicated plasmids toward the cell poles is similar to any of the two force-generating systems used by actin in eukaryotic cells. The DNA could move with the filaments of ParM via a treadmilling mechanism. The addition of new subunits to the ends of filaments may move the plasmid forward, a mechanism analogous to that occurring at the leading edge in amoeboid animal cells or in *Listeria monocytogenes* (Frishknecht and Way, 2001; Pantaloni *et al*., 2001). Alternatively, the ParM filaments could serve as a track on which motor proteins carry the plasmids to their destination, very much like the actin cytoskeleton, on which myosin moves its cargo. In either case, additional factors must be involved that determine the spatial organization of newly replicated plasmids and ensure directionality of plasmid distribution.

The crystallography and electron microscopy studies presented here show that ParM is a close relative of MreB and actin, both in its three-dimensional structure and in its propensity to form actin-like filaments. Actin has a variety of distinct roles in eukaryotic cells. MreB shares its role in the maintenance of cell shape. In contrast, ParM is required for plasmid partitioning, which adds a new function to bacterial actin-like filaments. A very interesting question raised by this finding is which of the force-generating mechanisms used by actin in eukaryotic cells is the basis for DNA partitioning in prokaryotes. The answer will provide us with important insights into this fundamental process in bacteria and may provide evidence for the prokaryotic ancestry of actin-based motility.

Materials and methods

Protein expression and purification

Native ParM (35.7 kDa) was overexpressed in *E.coli* BL21(DE3) cells (Stratagene) from pMD137 (Dam and Gerdes, 1994). The pMD137 plasmid vector contains the *parM* gene (SWISSPROT accession No. P11904) in front of an isopropyl-β-D-thiogalactopyranoside (IPTG)-inducible P*tac* promoter. Cells were grown at 30°C in 2× TY medium supplemented with 0.2% glucose and 50 μg/ml kanamycin until OD_{600} = 0.6, when protein expression was induced by addition of 1 mM IPTG. After 3 h of induction, the cells were harvested and frozen in liquid nitrogen. Cells were resuspended in lysis buffer (30 mM Tris–HCl pH 7.5, 25 mM KCl, 1 mM $MgCl_2$, 1 mM DTT, 0.1% Triton X-100) containing 0.2 mg/ml lysozyme and 5 μg/ml DNase I, and sonicated. The cell extract was cleared by centrifugation for 60 min at 100 000 *g* and ParM was precipitated by addition of ammonium sulfate to a final concentration of 10% (w/v). Precipitated protein was resuspended in buffer A (30 mM Tris–HCl pH 7.5, 25 mM KCl, 1 mM $MgCl_2$, 1 mM DTT). ParM was precipitated by addition of 10 mM $MgCl_2$ and 10 mM ATP, followed by immediate centrifugation for 15 min at 100 000 *g*. Remaining ParM protein in the supernatant was precipitated by a second addition of 10 mM ATP. This allowed high recovery of the protein at high purity. Finally, ParM was gel filtrated on a HiPrep Sephacryl S200 column (Amersham-Pharmacia) using buffer A. The protein, eluting as a single peak, was frozen in liquid nitrogen and stored at –80°C.

Electron microscopy and image processing

ParM filaments for electron microscopy were prepared by incubating 3.5 μM protein in polymerization buffer (30 mM Tris–HCl pH 7.5, 100 mM KCl, 2 mM $MgCl_2$, 1 mM DTT) with 2 mM ATPγS for 5 min at ambient temperature. Filaments were diluted 1:10 in polymerization buffer, applied to glow-discharged carbon-coated copper grids and negatively stained using 1% uranyl acetate. Electron microscopy was performed at 80 kV using a Philips EM208 transmission electron microscope. Images were photographed at a magnification of 32 000–50 000×. Images of single filaments, initially selected for their straightness and length, were digitized using a Zeiss SCAI CCD scanner at 7 μm resolution and compressed to 28 μm pixels. They were analysed using MRC image-processing software (Crowther *et al*., 1996). Filtered images were obtained by calculating Fourier transforms of straightened images (see Figure 2), masking off a box around each layer line and back-transforming. For three-dimensional reconstruction, data from nine layer lines, including the equator, were extracted from the Fourier transforms of filaments that gave good symmetrical patterns, and their phases and amplitudes were compared. The data from six best filaments, with a total length of ~3300 nm, were averaged after their phases had been adjusted to bring them into the same orientation. The resolution of the reconstructed image is ~32 Å.

SeMet-substituted ParM

SeMet-substituted ParM was expressed in BL21(DE3). Methionine biosynthesis was inhibited as described previously (Van Duyne *et al*., 1993). A preculture, grown in 2× TY medium with 50 μg/ml kanamycin, was used at 1000-fold dilution to inoculate 250 ml of M9 minimal medium supplemented with 0.4% glucose, 2 mM $MgSO_4$, 1 μg/ml thiamine and 50 μg/ml kanamycin. After growth overnight, the culture was diluted into 12 l of minimal medium and grown to an OD_{600} of 0.3, when 50 mg/l L-SeMet (Acros Organics), 50 mg/l leucine, isoleucine and valine, and 100 mg/l lysine, threonine and phenylalanine (Fluka) were added. After 15 min, IPTG (1 mM) was added to induce protein expression for 12 h at 30°C. SeMet-substituted ParM was purified as described for the native protein, except that 5 mM DTT was added to all solutions. The incorporation of SeMet was confirmed by electrospray ionization mass spectrometry [ParM observed 35 764.6 Da (calculated 35 765.6 Da); SeMet ParM observed 36 045.2 Da (calculated 36 046.9 Da)].

Crystallization and data collection

Crystals were grown by the sitting-drop vapor diffusion technique. Native and SeMet-substituted ParM protein crystallized in 1.4–1.6 M Na_3 citrate pH 6.5 and 80–100 mM guanidine–HCl. The SeMet crystals were improved by the addition of 0.6 μl of a 30 (w/v) solution of 6-aminocaproic acid to the 6 μl droplet. Droplets composed of one part ParM protein (10 mg/ml) and one part mother liquor were equilibrated at 19°C. Crystals belonged to space group $P2_12_12$ with two molecules per asymmetric unit. The crystals were flash frozen in mother liquor containing 12% glycerol. Native ParM co-crystallized with ADP in 100 mM Na cacodylate pH 6.2, 400 mM NaCl, 400 mM Mg acetate and 11% PEG 8000 at 4°C. Prior to crystallization, the protein (10 mg/ml) was mixed with 1 mM ADP and 1 mM $MgCl_2$. Crystals belonged to space group $P4_1$ with two molecules in the asymmetric unit. The crystals had a twinning fraction of 0.5 (twin operators h, –k, –l) and showed symmetry consistent with point group 422. Crystals were soaked in mother liquor containing 30% PEG 400 and frozen in liquid nitrogen.

A MAD dataset as well as a native high-resolution dataset (APO) were collected on beamline ID14-4 (ESRF, Grenoble, France). Diffraction data from a frozen ParM–ADP crystal were collected at beamline 14-2 (SRS, Daresbury, UK). Crystallographic data are presented in Table II.

Structure determination and refinement

All data were indexed and integrated with MOSFLM (Leslie, 1991) and data were further processed using the CCP4 package (CCP4, 1994). Eight selenium sites were found using the program SOLVE (Terwilliger and Berendzen, 1999). The remaining four selenium sites were located using SHARP (de la Fortelle and Bricogne, 1997) and the initial phases were calculated with MLPHARE and SOLOMON (Abrahams and Leslie, 1996). A first model was built manually into the 2.6 Å MAD electron density map using the program MAIN (Turk, 1992). With this model, the

2.3 Å native crystal structure was solved by molecular replacement in CNS (Brünger *et al*., 1998). The ADP–ParM crystal structure was solved by molecular replacement after deletion of residues 29–69 of subdomain IB. Patterson correlation refinement allowing movement of domains I and II was essential. As the crystals were perfectly twinned, no attempt was made to de-twin the data prior to molecular replacement. All structures were built in MAIN2000 and refined using CNS1.1. Refinement statistics are summarized in Table III. Coordinates have been deposited in the PDB, entry code 1MWK (Apo form) and 1MWM (ADP-bound form).

Supplementary data

Supplementary data are available at *The EMBO Journal* Online.

Acknowledgements

We thank Sew Peak-Chew for the mass spectrometry analyses and Thomas Leonard for critically reading the manuscript. J.M.-J. was financially supported by the Danish Biotechnology.

References

Abrahams,J.P. and Leslie,A.G.W. (1996) Methods used in the structure determination of bovine mitochondrial F-1 ATPase. *Acta Crystallogr. D*, **52**, 30–42.

Addinall,S.G. and Lutkenhaus,J. (1996) FtsZ-spirals and -arcs determine the shape of the invaginating septa in some mutants of *Escherichia coli*. *Mol. Microbiol.*, **22**, 231–237.

Austin,S. and Abeles,A. (1983) Partition of unit-copy miniplasmids to daughter cells.1. P1- and F-miniplasmids contain discrete, interchangeable sequences sufficient to promote equipartition. *J. Mol. Biol.*, **169**, 353–372.

Belmont,L.D., Orlova,A., Drubin,D.G. and Egelman,E.H. (1999) A change in actin conformation associated with filament instability after P-i release. *Proc. Natl Acad. Sci. USA*, **96**, 29–34.

Bi,E.F. and Lutkenhaus,J. (1991) FtsZ ring structure associated with division in *Escherichia coli*. *Nature*, **354**, 161–164.

Bork,P., Sander,C. and Valencia,A. (1992) An ATPase domain common to prokaryotic cell cycle proteins, sugar kinases, actin and Hsp70 heat shock proteins. *Proc. Natl Acad. Sci. USA*, **89**, 7290–7294.

Brünger,A. *et al*. (1998) Crystallography & NMR system: a new software suite for macromolecular structure determination. *Acta Crystallogr. D*, **54**, 905–921.

CCP4 (1994) The CCP4 Suite: programs for protein crystallography. *Acta Crystallogr. D*, **50**, 760–763.

Chen,X., Cook,R.K. and Rubenstein,P.A. (1993) Yeast actin with a mutation in the hydrophobic plug between subdomain-3 and subdomain-4 (L266D) displays a cold-sensitive polymerization defect. *J. Cell Biol.*, **123**, 1185–1195.

Crowther,R.A., Henderson,R. and Smith,J.M. (1996) MRC image processing programs. *J. Struct. Biol.*, **116**, 9–16.

Dam,M. and Gerdes,K. (1994) Partitioning of plasmid R1—10 direct repeats flanking the parA promoter constitute a centromere-like partition site parC, that expresses incompatibility. *J. Mol. Biol.*, **236**, 1289–1298.

de la Fortelle,E. and Bricogne,G. (1997) Maximum-likelihood heavy-atom parameter refinement for multiple isomorphous replacement and multiwavelength anomalous diffraction methods. *Macromol. Crystallogr. A*, **276**, 472–494.

Egelman,E.H. (2001) Molecular evolution: actin's long lost relative found. *Curr. Biol.*, **11**, R1022–R1024.

Engh,R.A. and Huber,R. (1991) Accurate bond and angle parameters for x-ray protein-structure refinement. *Acta Crystallogr. A*, **47**, 392–400.

Erickson,H.P. (1998) Atomic structures of tubulin and FtsZ. *Trends Cell Biol.*, **8**, 133–137.

Flaherty,K.M., Delucaflaherty,C. and McKay,D.B. (1990) 3-dimensional structure of the ATPase fragment of a 70k heat-shock cognate protein. *Nature*, **346**, 623–628.

Frishknecht,F. and Way,M. (2001) Surfing pathogens and the lessons learned for actin polymerization. *Trends Cell Biol.*, **11**, 30–38.

Galkin,V.E., VanLoock,M.S., Orlova,A. and Egelman,E.H. (2002) A new internal mode in F-actin helps explain the remarkable evolutionary conservation of actin's sequence and structure. *Curr. Biol.*, **12**, 570–575.

Gerdes,K., Larsen,J.E.L. and Molin,S. (1985) Stable inheritance of plasmid R1 requires two different loci. *J. Bacteriol.*, **161**, 292–298.

Gerdes,K., Moller-Jensen,J. and Jensen,R.B. (2000) Plasmid and chromosome partitioning: surprises from phylogeny. *Mol. Microbiol.*, **37**, 455–466.

Gordon,G.S. and Wright,A. (2000) DNA segregation in bacteria. *Annu. Rev. Microbiol.*, **54**, 681–708.

Hayward,S., Kitao,A. and Berendsen,H.J.C. (1997) Model-free methods of analyzing domain motions in proteins from simulation: a comparison of normal mode analysis and molecular dynamics simulation of lysozyme. *Proteins*, **27**, 425–437.

Heald,R. (2000) Motor function in the mitotic spindle. *Cell*, **102**, 399–402.

Holm,L. and Sander,C. (1993) Protein-structure comparison by alignment of distance matrices. *J. Mol. Biol.*, **233**, 123–138.

Holmes,K.C., Popp,D., Gebhard,W. and Kabsch,W. (1990) Atomic model of the actin filament. *Nature*, **347**, 44–49.

Ireton,K., Gunther,N.W. and Grossman,A.D. (1994) Spo0j is required for normal chromosome segregation as well as the initiation of sporulation in *Bacillus subtilis*. *J. Bacteriol.*, **176**, 5320–5329.

Jensen,R.B. and Gerdes,K. (1997) Partitioning of plasmid R1. The ParM protein exhibits ATPase activity and interacts with the centromere-like ParR–parC complex. *J. Mol. Biol.*, **269**, 505–513.

Jensen,R.B. and Shapiro,L. (1999) Chromosome segregation during the prokaryotic cell division cycle. *Curr. Opin. Cell Biol.*, **11**, 726–731.

Jensen,R.B., Lurz,R. and Gerdes,K. (1998) Mechanism of DNA segregation in prokaryotes: replicon pairing by parC of plasmid R1. *Proc. Natl Acad. Sci. USA*, **95**, 8550–8555.

Jones,L.J.F., Carballido-Lopez,R. and Errington,J. (2001) Control of cell shape in bacteria: helical, actin-like filaments in *Bacillus subtilis*. *Cell*, **104**, 913–922.

Kabsch,W. and Holmes,K.C. (1995) Protein motifs 2. The actin fold. *FASEB J.*, **9**, 167–174.

Kabsch,W., Mannherz,H.G., Suck,D., Pai,E.F. and Holmes,K.C. (1990) Atomic structure of the actin DNaseI complex. *Nature*, **347**, 37–44.

Koonin,E.V. (1993) A superfamily of ATPases with diverse functions containing either classical or deviant ATP-binding motif. *J. Mol. Biol.*, **229**, 1165–1174.

Kraulis,P.J. (1991) MOLSCRIPT: a program to produce both detailed and schematic plots of protein structures. *J. Appl. Crystallogr.*, **24**, 946–950.

Laskowski,R.A., MacArthur,M.W., Moss,D.S. and Thornton,J.M. (1993) Procheck—a program to check the stereochemical quality of protein structures. *J. Appl. Crystallogr.*, **26**, 283–291.

Leslie,A.G.W. (1991) *Recent Changes to the MOSFLM Package for Processing Film and Image Plate Data*. SERC Laboratory, Daresbury, Warrington, UK.

Löwe,J. and Amos,L.A. (1998) Crystal structure of the bacterial cell-division protein FtsZ. *Nature*, **391**, 203–206.

Löwe,J. and Amos,L.A. (1999) Tubulin-like protofilaments in Ca^{2+}-induced FtsZ sheets. *EMBO J.*, **18**, 2364–2371.

Merritt,E.A. and Bacon,D.J. (1997) Raster3D: photorealistic molecular graphics. *Macromol. Crystallogr. B*, **277**, 505–524.

Mohl,D.A. and Gober,J.W. (1997) Cell cycle-dependent polar localization of chromosome partitioning proteins in *Caulobacter crescentus*. *Cell*, **88**, 675–684.

Møller-Jensen,J., Jensen,R.B. and Gerdes,H. (2000) Plasmid and chromosome segregation in prokaryotes. *Trends Microbiol.*, **8**, 313–320.

Møller-Jensen,J., Jensen,R.B., Löwe,J. and Gerdes,K. (2002) Prokaryotic DNA segregation by an actin-like filament. *EMBO J.*, **21**, 3119–3127.

Netzer,W.J. and Hartl,F.U. (1998) Protein folding in the cytosol: chaperonin-dependent and -independent mechanisms. *Trends Biochem. Sci.*, **23**, 68–73.

Nicholls,A., Sharp,K.A. and Honig,B. (1991) Protein folding and association—insights from the interfacial and thermodynamic properties of hydrocarbons. *Prot. Struct. Func. Genet*. **11**, 281–296.

Niki,H. and Hiraga,S. (1998) Polar localization of the replication origin and terminus in *Escherichia coli* nucleoids during chromosome partitioning. *Genes Dev.*, **12**, 1036–1045.

Ogasawara,N. and Yoshikawa,H. (1992) Genes and their organization in the replication origin region of the bacterial chromosome. *Mol. Microbiol.*, **6**, 629–634.

Ogura,T. and Hiraga,S. (1983) Partition mechanism of F-plasmid: two plasmid gene-encoded products and a *cis*-acting region are involved in partition. *Cell*, **32**, 351–360.

Otterbein,L.R., Graceffa,P. and Dominguez,R. (2001) The crystal structure of uncomplexed actin in the ADP state. *Science*, **293**, 708–711.

Pantaloni,D., Le Clainche,C. and Carlier,M.F. (2001) Mechanism of actin-based motility. *Science*, **292**, 1502–1506.

Robinson,R.C., Turbedsky,K., Kaiser,D.A., Marchand,J.B., Higgs,H.N., Choe,S. and Pollard,T.D. (2001) Crystal structure of Arp2/3 complex. *Science*, **294**, 1679–1684.

Rothfield,L., Justice,S. and Garcia-Lara,J. (1999) Bacterial cell division. *Annu. Rev. Genet.*, **33**, 423–448.

Sablin,E.P., Dawson,J.F., VanLoock,M.S., Spudich,J.A., Egelman,E.H. and Fletterick,R.J. (2002) How does ATP hydrolysis control actin's associations? *Proc. Natl Acad. Sci. USA*, **99**, 10945–10947.

Schutt,C.E., Myslik,J.C., Rozycki,M.D., Goonesekere,N.C.W. and Lindberg,U. (1993) The structure of crystalline profilin β-actin. *Nature*, **365**, 810–816.

Sharpe,M.E. and Errington,J. (1999) Upheaval in the bacterial nucleoid—an active chromosome segregation mechanism. *Trends Genet.*, **15**, 70–74.

Terwilliger,T.C. and Berendzen,J. (1999) Automated MAD and MIR structure solution. *Acta Crystallogr. D*, **55**, 849–861.

Turk,D. (1992) Weiterentwicklung eines Programms für Molekülgrafik und Elektrondichte-Manipulation und seine Anwendung auf verschiedene Protein-Strukturaufklärungen. PhD thesis, Technical University of Munich, Munich, Germany.

van den Ent,F. and Löwe,J. (2000) Crystal structure of the cell division protein FtsA from *Thermotoga maritima*. *EMBO J.*, **19**, 5300–5307.

van den Ent,F., Amos,L.A. and Löwe,J. (2001a) Prokaryotic origin of the actin cytoskeleton. *Nature*, **413**, 39–44.

van den Ent,F., Amos,L. and Löwe,J. (2001b) Bacterial ancestry of actin and tubulin. *Curr. Opin. Microbiol.*, **4**, 634–638.

van Duyne,G.D., Standaert,R.F., Karplus,P.A., Schreiber,S.L. and Clardy,J. (1993) Atomic structures of the human immunophilin Fkbp-12 complexes with Fk506 and rapamycin. *J. Mol. Biol.*, **229**, 105–124.

Received August 20, 2002; revised October 4, 2002; accepted October 22, 2002